2020 IEEE 20th International Conference on Nanotechnology (IEEE-NANO)
July 29-31 2020, Virtual Conference

Single Electron Control by a Uniform Magnetic Field in a Focusing Double-Well Potential Structure

Mauro Ballicchia[1], Mihail Nedjalkov[1], and Josef Weinbub[2,*]

Abstract— **Double-well potential structures provide rich capabilities for single electron control via different physical characteristics of the potentials and the electron state. Here, we investigate the effect of a uniform magnetic field on the electron state interference pattern manifesting in a focusing double-well potential structure by conducting Wigner quantum transport experiments. We analyze the electron density and the negativity of the Wigner function and show how the magnetic field controls the electron state but also destroys the coherence of the evolution dynamics. Our work contributes to the fundamental understanding of magnetic field based single electron control mechanisms and sheds light on the critical decoherence processes.**

I. INTRODUCTION

To this day, the Young double-slit experiments play a fundamental role to provide insights into the quantum properties of photons [1], electrons [2], and molecules [3].

From a probabilistic point of view the double-slit experiment comprises a number of independent identical trials of the interaction of an object, e.g., an electron, with a detector, e.g., a screen, placed behind a potential wall with two slits. The potential wall is sufficiently high and wide to block other paths of the electron except through the two slits. Identical trials refer to equivalent physical conditions of all trials, in particular the initial position and momentum of all launched electrons are the same. The independence of the trials requires that the experiments are uncorrelated: The electrons from the consecutive trials cannot interact. This means that in a conventional laboratory experiment the time intervals between the trials must be large enough to avoid Coulomb interaction [4]. However, there are no other limitations of the consecutive trials, e.g., no requirement for a constant time period between trials. On the contrary, in a simulation experiment the time can be arbitrarily small, provided that the electrons are treated as non-interacting; it is convenient (but technically not necessary) to initialize the consecutively injected electrons periodically in time. After each interaction with the screen a single electron leaves a well-localized mark. After many trials the distribution of the marks shows a well-pronounced pattern of alternating minima and maxima, demonstrating the quantum (i.e., wave) character of the electron.

Young-type experiments establish the foundations for advanced interference based applications, e.g., electron control for information processing [5][6] and entangletronics [7]. Alternatively, electron control can be established by specifically shaped electric potentials, called lenses [8]: Electron state splitting [7] or focusing has been investigated [9]. These splitting or focusing mechanisms are quantum phenomena based on interference effects, used to, e.g., improve the device performance. Based on investigations of single potential structures [10], it has been recently observed that the operation of such lenses can be realized by two potential wells, for example, provided by a double-dopant setup [11]. A well-pronounced interference pattern was observed, similar to the double-slit experiment but without the need for a conventional double-slit potential [12]. The process has been further investigated regarding the effect of different physical settings, such as the distance between the dopants, their potential, and various initial electron states.

In this work, we report the interplay of the manifesting interference pattern with an applied uniform magnetic field in a focusing double-well potential structure placed in a quantum wire. We utilize the Wigner quantum transport simulator VIENNAWD [13] to investigate the electron density and Wigner function negativity. The latter provides insights into the quantum character of the evolution, in particular, into interference effects and is a unique feature of the Wigner transport picture not provided by other quantum transport models (e.g. based on wave mechanics) [14][15]. Single electron magnetic control is attractive for quantum information processing and advanced sensors [5].

II. WIGNER TRANSPORT MODEL

We consider the evolution of an initial electron state described by the Wigner function f_w in a two-dimensional phase space $\mathbf{r} = x, y$; $\mathbf{p} = k_x, k_y$ in presence of a magnetic field $\mathbf{B}$ [16]. The evolution equation for the Wigner function is

$$\left[\frac{\partial}{\partial t} + \frac{\mathbf{p}}{m}\cdot\frac{\partial}{\partial \mathbf{r}} + e\frac{\mathbf{p}}{m}\times\mathbf{B}\cdot\frac{\partial}{\partial \mathbf{p}}\right] f_w(\mathbf{p},\mathbf{r},t) = \int d\mathbf{p}' V_w(\mathbf{p}-\mathbf{p}',\mathbf{r}) f_w(\mathbf{p}',\mathbf{r},t)\,. \quad (1)$$

The equation is *not* an approximation obtained by introducing the magnetic component of the Lorentz force in analogy with the classical (Boltzmann) equation. Indeed, it is an exact quantum-coherent model obtained from the general magnetic Wigner theory [16] for the case of a spatially-dependent but near stationary electric field $\mathbf{E}(\mathbf{r})$ and a constant magnetic field $\mathbf{B}$. The gauge invariance of the problem is demonstrated by the fact that the integral on the right-hand side can be equivalently expressed by means of $\mathbf{E}(\mathbf{r})$ [16].

[1]Institute for Microelectronics, TU Wien, Austria.
[2]Christian Doppler Laboratory for High Performance TCAD, Institute for Microelectronics, TU Wien, Austria.
Corresponding author: J. Weinbub
josef.weinbub@tuwien.ac.at

In particular the electric component **E** of the Lorentz force, embodied in the Wigner potential V_w, is obtained in the limit of homogeneous electric conditions. Equation (1) becomes independent from the electromagnetic potentials and thus from the choice of a particular gauge, enabling gauge-independent numerical approaches. The equation has been associated with a stochastic computational model based on the fact that a maximum coherence length **L** may be specified in nanostructures, which limits the range of the standard Weyl transform [17]. As a result, the momentum space becomes quantized.

The numerical Monte Carlo theory for solving integral equations [18] has been applied to the integral form of (1). A set of stochastic concepts and notions has been derived and unified into the Wigner signed particle model [19]. In particular, a given Wigner state (representing an electron) is represented by numerical particles which carry a sign during the evolution, thus constituting *signed particles*. The signed particles contribute to the statistics of the physical averages in the same way as classical Boltzmann particles, however, their contribution is multiplied by the carried sign in the quantum Wigner counterpart. The signed particles are accelerated by the magnetic force over Newtonian trajectories in the classical way, while the action of the Wigner potential V_w gives rise to generation of new signed particles. Both the generation rate and the distribution of momentum are determined by the Wigner potential. An important property is that two signed particles with opposite sign that meet in a cell of the phase space at the same time annihilate each other. This aspect gives rise to the concept of indistinguishable particles, which are stored on a phase space grid at consecutive time steps, so that a number per phase space grid cell replaces the ensemble of particle states within that cell. Applying this concept greatly reduces the memory requirements in the implementation of the model: Wigner simulations of multi-dimensional structures became only possible because of this and is also applied in ViennaWD.

III. Simulation Analysis

Fig. 1 shows the details of the geometry of the simulated quantum wire defined by infinite potentials along the left and right boundary as well as the averaged electron density distribution for symmetrically-sized potential wells and no magnetic field. The boundaries in the vertical transport direction (from bottom to top) are open. Green isolines at 0.175 eV indicate the two Coulomb potential wells. The initial state of the electron is the Wigner function corresponding to a minimum uncertainty wave packet with a standard deviation of $\sigma = 8\,\mathrm{nm}$. The central wave vector is $(k_{0x}, k_{0y}) = (0, 0.837\,\mathrm{nm}^{-1})$ and corresponds to an energy of 0.14 eV. The initial state is centered at ($x = 10\,\mathrm{nm}$, $y = 0\,\mathrm{nm}$) and is injected at the bottom boundary, directed upwards towards the wells. Any injection of such a state resembles an independent, identically distributed trial in Young's double-slit experiment. As hinted in Section I, the simulation experiment offers the opportunity to inject (each femtosecond) a novel state without biasing the result, because the Coulomb interaction between the injected electrons is suppressed.

The averaged statistics in Fig. 1 shows the induced interference with a strongly pronounced compression of the electron density in the middle upper part: The wells act as a lense (i.e., focusing effect), which is presented by a high density peak between $y = 20\,\mathrm{nm}$ and $y = 25\,\mathrm{nm}$. In the considered case of a disabled magnetic field, the pattern reflects the symmetry of the experimental setup. These considerations are confirmed in Fig. 2, obtained by reducing the potential of the left well by 50%. This shows how the interference pattern can be manipulated by a well-induced electric field. Similar behavior is observed if the magnetic field is enabled: Fig. 3 corresponds to the symmetric double-well potential case with an applied magnetic field of $B = -6\,\mathrm{T}$. The magnetic field shifts the density peak in a way which resembles the action of the asymmetric lense shown in Fig. 2. Both effects, the magnetic field and the asymmetric potentials, can be combined to work in tandem to further shift the peak to the right, see Fig. 4.

However, despite the similarity of the electric and magnetic effects on the quantum electron density distribution, we observe that the electric and magnetic fields play a very different role in the transport dynamics. Fig. 5 and Fig. 6 present the Wigner function negativity maps for $B = 0$ and $B = -6\,\mathrm{T}$, respectively. Having in mind the property of the Wigner function to develop negative values in the regions of quantum interference [14], the maps $f_w^-(x,y)$ are created by integrating the negative values of the corresponding Wigner functions over the momentum coordinates. As Fig. 6 clearly shows, the magnetic field destroys the coherence of the dynamics as the negativity is drastically reduced. This can be linked to the role of the two responsible electromagnetic terms in (1). In terms of particle trajectories, the Lorentz force depends directly on **p**. The effect of the electric counterpart is smoothed by the integral on the momentum. A heuristic understanding is given by the stochastic interpretation of the Wigner evolution as an ensemble of signed particles, where the sign carries the quantum information. However, the particle dynamics follows the Boltzmann evolution: Particles follow Newtonian trajectories, which are accelerated only by (i) the magnetic field in the case of a general electric potential, giving rise to the Wigner potential in (1), or by (ii) the Lorentz force in the case of electric potentials with up to quadratic spatial dependence (when the integral on the right-hand side of (1) reduces to the electric force **E**). In the latter case, the action of **E** is independent from the particle momentum so that the particles in the ensemble are accelerated synchronously. On the contrary, the action of **B** explicitly depends on **p**, which distorts the evolution.

IV. CONCLUSIONS

Interference effects offer rich opportunities for novel device operation principles based on the quantum character of the electron evolution on the nanometer scale. Double-well potential structures reveal a rich ability for controlling the manifesting interference pattern via different physical characteristics of the applied potentials and the electron state. Here, we investigate the interplay between the manifesting interference pattern and an applied uniform magnetic field and the relevance of the latter for quantum manipulation. Despite that the magnetic field works in tandem with the electric force, the effects of the two physical factors is very different: The magnetic field reduces the coherence, as demonstrated by the significantly reduced negativity of the Wigner function. A physical insight into the difference of the electric and magnetic actions is provided by the signed particle model, and is related to the dependence of the magnetic force on the particle momenta.

ACKNOWLEDGMENT

The financial support by the Austrian Science Fund (FWF): P29406 and P33609, the Austrian Federal Ministry for Digital and Economic Affairs, and the National Foundation for Research, Technology and Development is gratefully acknowledged. The computational results presented have been achieved using the Vienna Scientific Cluster (VSC).

REFERENCES

[1] P. Kolenderski, *et al.*, "Time-Resolved Double-Slit Interference Pattern Measurement with Entangled Photons," *Scientific Reports*, vol. 4, no. 1, p. 4685, 2014.
[2] R. Bach, *et al.*, "Controlled Double-Slit Electron Diffraction," *New Journal of Physics*, vol. 15, p. 033018, 2013.
[3] O. Nairz, *et al.*, "Quantum Interference Experiments with Large Molecules," *American Journal of Physics*, vol. 71, pp. 319–325, 2003.
[4] A. Tonomura, *et al.*, "Demonstration of Single-Electron Buildup of an Interference Pattern," *American Journal of Physics*, vol. 57, pp. 117–120, 1989.
[5] C. Bäuerle, *et al.*, "Coherent Control of Single Electrons: A Review of Current Progress," *Reports on Progress in Physics*, vol. 81, p. 056503, 2018.
[6] B. Marques, *et al.*, "Double-Slit Implementation of the Minimal Deutsch Algorithm," *Physical Review A*, vol. 86, p. 032306, 2012.
[7] P. Ellinghaus, *et al.*, "Analysis of Lense-Governed Wigner Signed Particle Quantum Dynamics," *Physica Status Solidi RRL*, vol. 11, p. 1700102, 2017.
[8] S. Chen, *et al.*, "Electron Optics with p-n Junctions in Ballistic Graphene," *Science*, vol. 353, pp. 1522–1525, 2016.
[9] P. Ellinghaus, *et al.*, "Improved Drive-Current into Nanoscaled Channels using Electrostatic Lenses," in *Proceedings of the International Conference on Simulation of Semiconductor Processes and Devices (SISPAD)*, 2015, pp. 24–27.
[10] M. Ballicchia, *et al.*, "Electron Evolution Around a Repulsive Dopant in a Quantum Wire: Coherence Effects," *Nanoscale*, vol. 10, pp. 23 037–23 049, 2018.
[11] J. Weinbub, *et al.*, "Electron Interference in a Double-Dopant Potential Structure," *Physica Status Solidi RRL*, vol. 12, p. 1800111, 2018.
[12] H. Hongo, *et al.*, "A 40-nm-Pitch Double-Slit Experiment of Hot Electrons in a Semiconductor Under a Magnetic Field," *Applied Physics Letters*, vol. 70, pp. 93–95, 1997.
[13] "ViennaWD: Wigner Decoherence Simulator." [Online]. Available: www.iue.tuwien.ac.at/software/viennawd/
[14] J. Weinbub *et al.*, "Recent Advances in Wigner Function Approaches," *Applied Physics Reviews*, vol. 5, p. 041104, 2018.
[15] M. Ballicchia, *et al.*, "Investigating Quantum Coherence by Negative Excursions of the Wigner Quasi-Distribution," *Applied Sciences*, vol. 9, p. 1344, 2019.
[16] M. Nedjalkov, *et al.*, "Wigner Equation for General Electromagnetic Fields: The Weyl-Stratonovich Transform," *Physical Review B*, vol. 99, p. 014423, 2019.
[17] P. Ellinghaus, "Two-Dimensional Wigner Monte Carlo Simulation for Time-Resolved Quantum Transport with Scattering," Doctoral Dissertation, TU Wien, 2016. [Online]. Available: http://www.iue.tuwien.ac.at/phd/ellinghaus/
[18] M. Nedjalkov, *et al.*, "Unified Particle Approach to Wigner-Boltzmann Transport in Small Semiconductor Devices," *Physical Review B*, vol. 70, no. 11, p. 115319, 2004.
[19] D. K. Ferry *et al.*, *The Wigner Function in Science and Technology*. Bristol, UK: IoP Publishing, 2018.

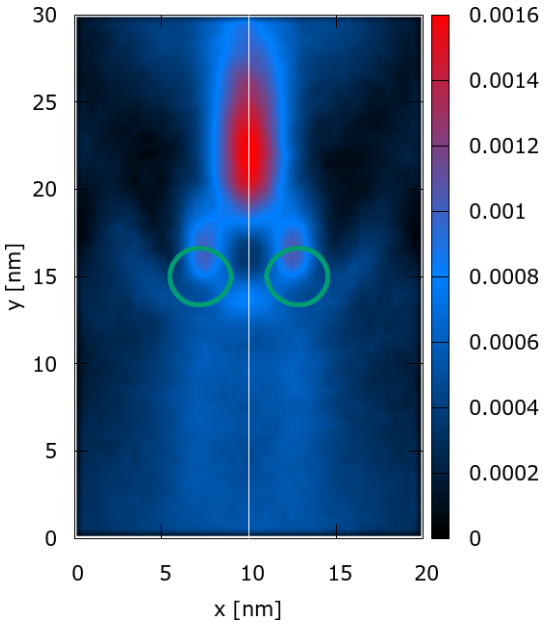

Fig. 1. Electron density distribution (arb. unit) obtained for a symmetric double-well potential with no magnetic field applied ($B = 0$).

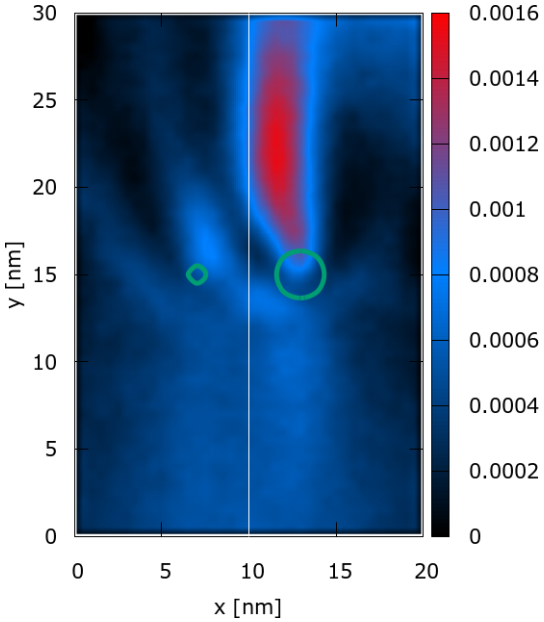

Fig. 2. Electron density distribution (arb. unit) obtained for an asymmetric double-well potential with no magnetic field applied ($B = 0$).

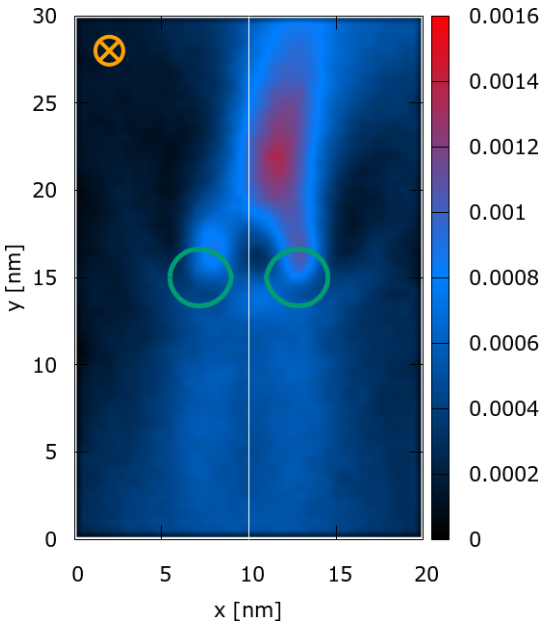

Fig. 3. Electron density distribution (arb. unit) obtained for a symmetric double-well potential and $B = -6\,\mathrm{T}$

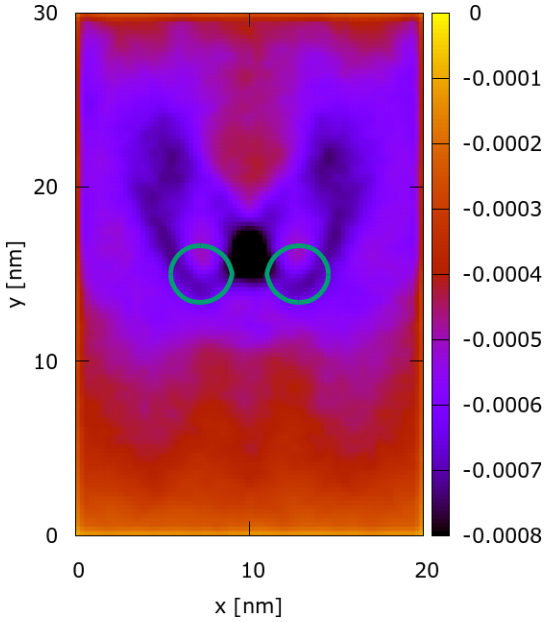

Fig. 5. Wigner function negativity map, symmetric double-well potential ($B = 0$).

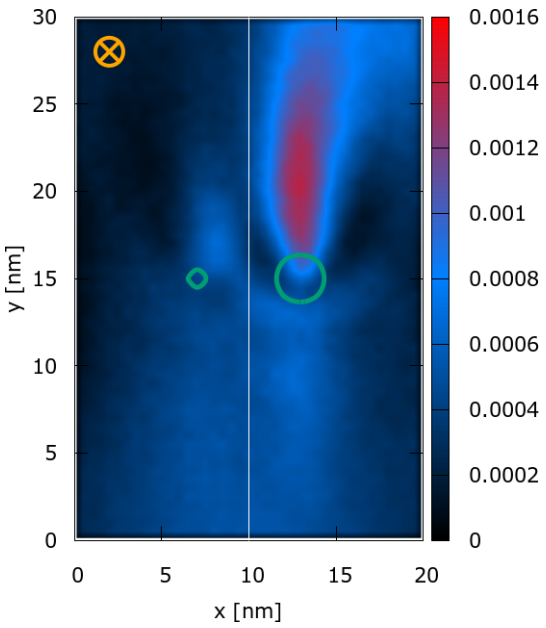

Fig. 4. Electron density distribution (arb. unit) obtained for an asymmetric double-well potential and $B = -6\,\mathrm{T}$.

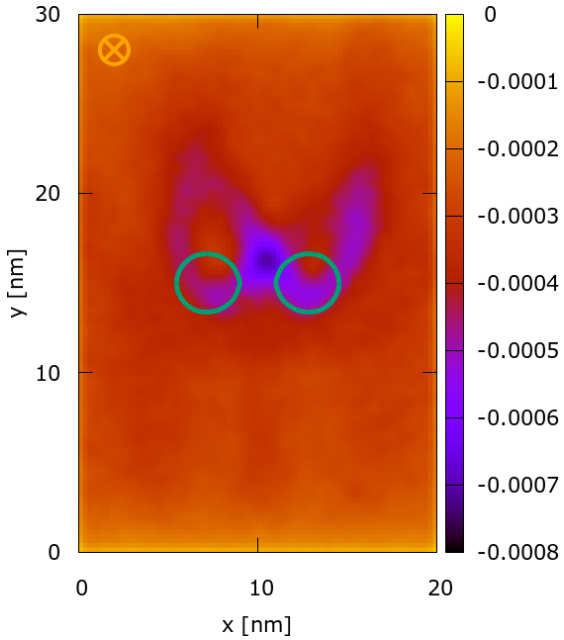

Fig. 6. Wigner function negativity map, symmetric double-well potential ($B = -6\,\mathrm{T}$).